Alexandria Engineering Journal 86 (2024) 584–590

Contents lists available at ScienceDirect

Alexandria Engineering Journal

journal homepage: www.elsevier.com/locate/aej

ORIGINAL ARTICLE

Cost-effective and highly accurate antenna with built-in calibration for V2X communications

Sol Kim [a,1], Hyun-Jun Dong [b], Han Lim Lee [b,*]

[a] School of Electrical Engineering, Korea Advanced Institute of Science and Technology (KAIST), Daejeon, 34141, South Korea
[b] School of Electrical and Electronics Engineering, Chung-Ang University, Seoul, 06974, South Korea

ARTICLE INFO

Keywords:
Minimum vector-sum
On-board calibration
Phased array systems
Built-in calibration

ABSTRACT

This paper presents a phased array system (PAS) with built-in calibration to reduce cost and improve the accuracy for vehicle-to-everything (V2X) communications. Unlike other high-complexity and high-cost calibration methods, our proposed built-in calibration achieves a lower cost and low complexity by detecting only the magnitude. Conventional built-in calibration uses a mixer, thus causing high power consumption and high cost. However, our proposed built-in calibration method searches for the minimum of the vector-sum point from the signal by sampled lines on-board, resulting in a higher accuracy. The vector-sum point goes to a minimum when the phase and magnitude are in balance. Therefore, the phase and magnitude imbalance can be easily monitored by controlling phase shifters and attenuators in PAS. To verify our proposed built-in calibration in PAS, a T/Rx with four RF-chains and sampled lines was fabricated at 5.8 GHz. Its performance was then demonstrated through simulated and measured results. Moreover, a communication performance evaluation using an actual vehicle was performed both before and after calibration. As a result, we found that a signal without distortion was transmitted after calibration.

1. Introduction

As interest in autonomous driving continues to grow, the demand for vehicle-to-everything (V2X) communication has increased rapidly. V2X communication is a crucial technique in modern transportation systems and requires the use of phased array systems (PASs) to facilitate communication [1]. These PASs are able to send and receive signals from a moving vehicle while also receiving signals from other sources that may also be in motion [2].

In V2X communication, PASs are employed to enhance efficiency and transmission performance. A key factor in achieving this is the use of beamforming techniques [3–7], whose performance is determined by the radiation field characteristics generated by each antenna element [8,9]. As such, it is imperative that the phase and magnitude of each element are balanced or the radiation pattern of the PAS may be adversely affected by an inappropriate side lobe. Therefore, calibration is necessary to ensure efficient beamforming [10,11].

Several calibration methods for PASs have been researched, which can broadly be divided into off-board and on-board types. In the off-board type methods, the system or instrument is calibrated outside of the device using external equipment or tools. This includes far-field or near-field calibration [12–20], which are based on monitoring the maximum power received from the antenna at a far-field or near-field reference point. Off-board types are suitable for calibrating factory default settings, not periodic calibration, because it requires a reference antenna to measure the received power.

PASs used in vehicles not only require factory-level calibration but also calibration after shipment. The performance of a PAS can change over time due to variations in the temperature range inside a vehicle [21,22]; thus, periodic calibration is necessary, making built-in calibration of the on-board type necessary [23]. On-board calibration is performed using peripheral fixed probes, mutual probes, or sampled lines. The peripheral fixed probe method corrects errors by inserting probes between antennas [12,24], while the mutual probe method can correct errors without additional antennas [12,25–27]. However, the two methods struggle to accurately distinguish signals from each radio frequency (RF) chain; therefore, the algorithm becomes complicated and the calibration accuracy is low. The sampled line method is simple to calibrate because the coupled signal is ideally identical across all RF-chains [28–31].

* Corresponding author.
E-mail addresses: k.sol@kaist.ac.kr (S. Kim), dongssl@hanwha.com (H.-J. Dong), hanlimlee@cau.ac.kr (H.L. Lee).
[1] This is the first author.

https://doi.org/10.1016/j.aej.2023.12.017
Received 19 June 2023; Received in revised form 16 October 2023; Accepted 10 December 2023
Available online 14 December 2023

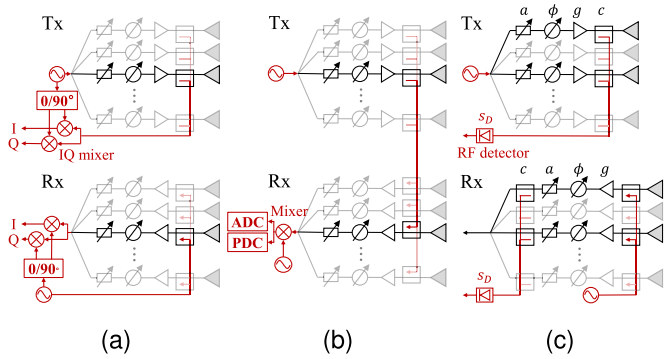

Fig. 1. Schematic diagram of on-board built-in calibration using sampled lines: with a conventional (a) IQ mixer, (b) loopback scheme, and (c) proposed RF detector.

Fig. 1 (a) and (b) show conventional built-in calibration methods with sampled lines. In Fig. 1 (a), the beamforming transmitter and receiver can calibrate by detecting the phase and amplitude of each RF-chain using an IQ mixer [32–36]. However, it requires IQ mixers, which cannot avoid IQ mismatch and power consumption. Fig. 1(b) shows the form of a closed-loop of a transceiver and the IQ mixer replaced by using a mixer [37,38]. For example, the phase and amplitude of the 2nd Rx RF-chain can be relatively compared for the 3rd Rx RF-chain calibration with the 3rd Tx in operation. However, a mixer is still required, and RF paths for loop formation increase in complexity. Active elements required in conventional methods increase power consumption and cost. To solve this, a new built-in on-board type calibration is needed. The aforementioned characteristics of state-of-the-art phased arrays with the calibrations are summarized in Table 1.

In this study, we replace the mixer with an RF detector, as shown in Fig. 1 (c), and propose built-in calibration by detecting only the magnitude. The use of RF detectors has a low cost because power consumption is low and inexpensive. However, using only magnitude provides low accuracy for calibration [20,39–43]. This is because the change in magnitude is low near the maximum received power, making it difficult to detect the change. We propose a new built-in calibration that improves accuracy while simultaneously achieving a low cost.

The contributions of this paper are summarized as follows:

1. The proposed built-in calibration is based solely on a comparison of the signal sampled by the main RF path in an on-board type as shown in Fig. 1 (c). Therefore, it does not require an additional reference antenna or detecting probe.
2. The proposed method monitors only magnitude on-board, achieving a lower cost and higher accuracy using the minimum vector-sum than the conventional method.
3. The proposed system allows for periodic calibration after shipment in addition to factory initial settings by configuring the calibration in an on-board type method.
4. To verify the proposed built-in calibration, beam patterns and communication performance in vehicles are compared before and after calibration.

Section 2 presents the proposed built-in calibration methodology, including how to calibrate the phase and magnitude for low cost and improved accuracy. In addition, the design of the proposed built-in calibration is explained and simulation results comparing performance before and after calibration are provided. In Section 3, the system configuration and experimental environment are described and experimental results are compared before and after calibration. Finally, Section 4 presents the discussion and conclusion of this work.

Table 1
Comparison of state-of-the-art phased arrays with calibration.

	[20]	[28]	[38]	This work
Method	Far-field	Mutual Probe	Sampled Line	Proposed
Periodicity	X	O	O	O
Cost Efficiency	O	O	X	O
Accuracy	Low	Low	High	High

2. Proposed built-in calibration

2.1. Methodology

Fig. 1 shows the configuration of the antenna, amplifier, phase shifter, and attenuation for each channel, where two arbitrarily selected RF-chains with sampled lines are coupled and compared. When the same magnitude (α) and phase (ϕ) are fed to two sampled lines, the detected signal of the RF detector goes to the maximum. Contrarily, the minimum (or null) is generated if the signal is fed to two sampled lines with a 180° phase difference. The detected signal (s_D) from p-th and q-th RF-chains can be simply expressed by magnitude and phase as follows:

$$\begin{aligned} s_D &= c_p g_p a_p e^{-j\phi_p} + c_q g_q a_q e^{-j\phi_q} \\ &= \alpha_p e^{-j\phi_p} + \alpha_q e^{-j\phi_q}, \end{aligned} \tag{1}$$

where c, g, a, α, and ϕ denote the coupling coefficient (a measure of how much power is transferred between the main RF line and sampled line), channel gain, attenuation level, magnitude, and phase by the RF-chains, respectively. In the case of the conventional method, we simply assume that $\phi_p = \phi_q = 0°$ in (1). (2) calculates the detected signal of the conventional method to the maximum as

$$s_D = \alpha_p e^{-j0} + \alpha_q e^{-j0} = \alpha_p + \alpha_q. \tag{2}$$

The proposed method is based on the detected signal, which combines two selected antenna element signals with a 180° phase difference. Therefore, in the case of the proposed method, simply assume that $\phi_q = \phi_p + \pi$ and $\phi_p = 0°$ in (1). The detected signal goes to null where the magnitude of the arbitrary signals is the same in (3):

$$s_D = \alpha_p e^{-j0} + \alpha_q e^{-j\pi} = \alpha_p - \alpha_q. \tag{3}$$

To design this, we have the sampled lines with a 180° phase difference in front of the RF detector, as shown in Fig. 1 (c). Then, the detected signal in the RF detector has the minimum values, as shown in (3).

When there is phase and magnitude imbalance, the change (ΔS_D) of S_D (log scale of s_D) means the accuracy of the calibration. This is because it is difficult to detect if the change in S_D is small when it is imbalanced, so the accuracy of calibration is inevitably low. Assume $\alpha_p = \alpha_q = 1$, and $\phi_p = 0$. Then, the phase imbalance ($|\phi_p - \phi_q|$) with ϕ_q as a variable is expressed. $\Delta S_D(\phi_q)$ is expressed as (4):

$$\Delta S_D(\phi_q) = S_D(\phi_q) - S_D(\phi_q - \Delta\phi), \tag{4}$$

where $\Delta\phi$ means the amount of phase change and $\Delta\phi = 1°$ in this paper. The magnitude imbalance can also be analyzed in the same way. Assume $\phi_p = \phi_q = 0$, and $\alpha_p = 1$. Then, the magnitude imbalance ($|\alpha_p - \alpha_q|$) with α_q as a variable is expressed. $\Delta S_D(\alpha_q)$ is expressed as (5):

$$\Delta S_D(\alpha_q) = S_D(\alpha_q) - S_D(\alpha_q - \Delta\alpha), \tag{5}$$

where $\Delta\alpha$ is the magnitude change, and in this paper, $\Delta\alpha = 0.01$. Calibration is the process of comparing a reference element and adjusting

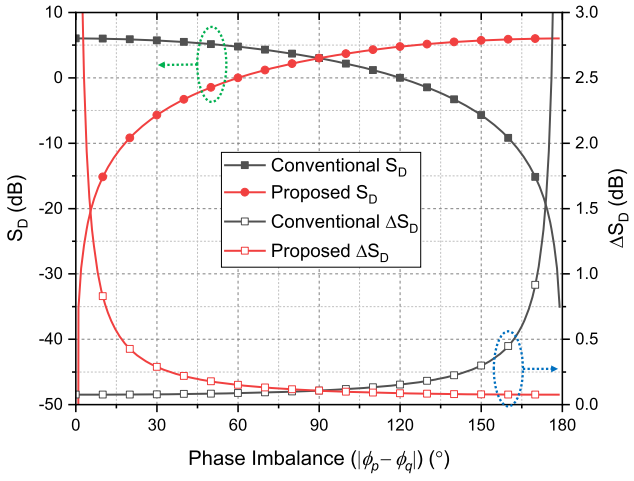

(a)

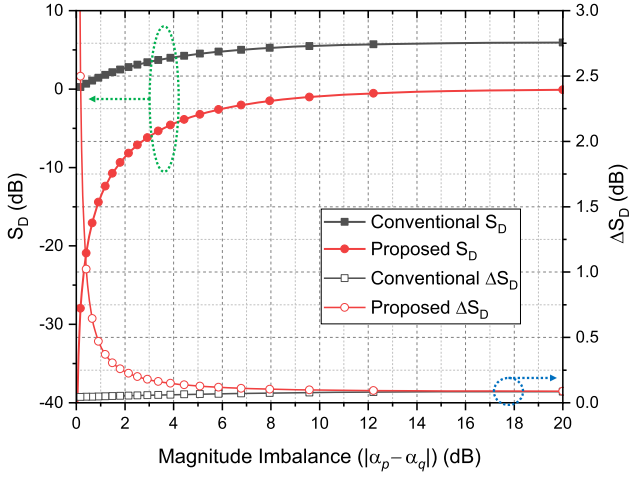

(b)

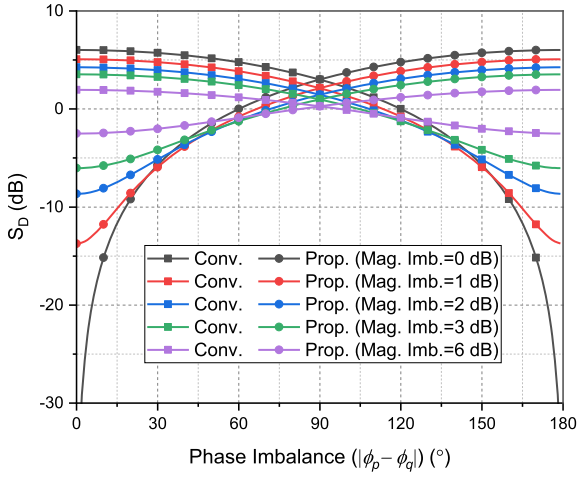

(c)

Fig. 2. Comparison of detected signals and changes between the conventional and the proposed method using the magnitude of two RF-chains: (a) phase imbalance and (b) magnitude imbalance. (c) Null depth by magnitude imbalance.

for balance. When the change (ΔS_D) near a goal point between the reference and comparison elements is small and cannot be observed, high sensitivity is required to detect the change as shown in Fig. 2. Conversely, if the change (ΔS_D) around the goal point is large, accurate calibration is possible. Thus, calibration for maximum directivity gain, as shown in Fig. 1 (c), is more difficult than monitoring the minimum (or null). The proposed method based on the conventional method utilizes a minimum point to improve accuracy. The purpose of the phased array calibration is that the phase and magnitude of the arbitrary signals are well balanced; thus, the imbalances are easily detected by tracking the minimum from the proposed built-in calibration, as shown in Fig. 2.

The calibration of phase and magnitude is divided into two steps. Firstly, when calibrating two RF-chains, the RF-chains are divided into a reference role and a swept role. In a swept RF-chain, the phase is compared with the phase of the reference RF-chain as it travels from 0 degrees to 360 degrees. As shown in Fig. 2 (a), the conventional method shows little change in ΔS_D near the target phase imbalance of 0 degree; therefore, fine calibration is difficult. However, the proposed method has a large ΔS_D near the target phase imbalance of 0 degree so fine calibration can be carried out. Phase balance can ultimately be found by measuring null according to the phase change, as shown in Fig. 2 (a). Next, the magnitude balance can easily be found once the phase errors are diagnosed. Thus, the magnitude of attenuation is controlled to determine the magnitude imbalance. The magnitude balance can be decided when null goes to a minimum according to magnitude change, as shown in Fig. 2 (b). In other words, as shown in Fig. 2 (c), the depth of the minimum value (or null) changes in the detected signals by 10 magnitude imbalances. The proposed calibration method can distinguish and calibrate imbalances in the phase and magnitude through the location and depth of the null. After phase calibration, the S_D change for magnitude imbalances is larger in the proposed method than in the conventional method; therefore, fine calibration can be carried out. The reason for guiding this process is that if the phase imbalance is excessively large (e.g. 50 degree), adjusting the attenuator will not significantly change the detected signal. During phase calibration, we do not leave as much as 50 degrees of phase imbalance. In the case of a 6-bit phase shifter, a maximum of 5.625 degrees of phase imbalance can occur. Unlike conventional methods, our proposed method can be performed with only the detected magnitude. In this way, the proposed method has an RF power detector instead of an additional detecting antenna or probe, or mixers. Therefore, the proposed built-in calibration has low cost and improved accuracy.

2.2. Design of built-in calibration

In Fig. 3, the PAS with the proposed built-in calibration consists of three zones: the RF driver, T/Rx beamforming chain, and detection & calibration. The RF drivers are designed to adjust the power level in both the transmitter and receiver modes. The RF signal output is transmitted through the RF divider to the beamforming chains in transmitter mode. Contrarily, the RF signal input is received from the RF combiner in receiver mode. The T/Rx beamforming chains consist of attenuators and phase shifters which cause errors in the PAS. When the balance of the signal fed to each antenna element is distorted, the radiation pattern of the phased array antenna is declined such as an unnecessary side-lobe. To address these issues, we propose the built-in calibration in PAS.

The proposed PAS is designed to operate in transmitter mode and receiver mode by the switch operation. The zone of detection and calibration is configured with switches, and sampled lines, which have a 180° phase difference ($=\lambda/2$). The switches are adopted to select the operation mode and calibration paths. Fig. 3 shows the proposed operations in both the transmitter and receiver modes. For example, if the switches connect the transmitter path of antenna 2 and antenna 4, the two signals are compared on-board. Because the signals are given through the sampled lines, there is an advantage that the main signal

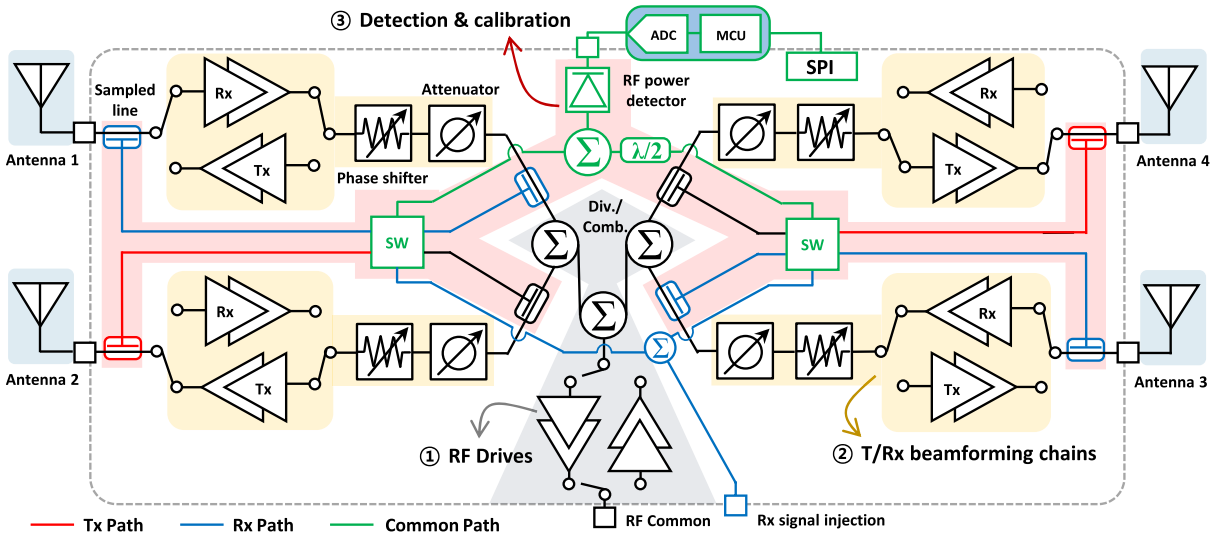

Fig. 3. Diagram in transmitter mode and receiver mode of the proposed built-in calibration. For example, antennas 2 and 4 in transmitter mode, and antennas 1 and 3 in receiver mode are calibrating on-board.

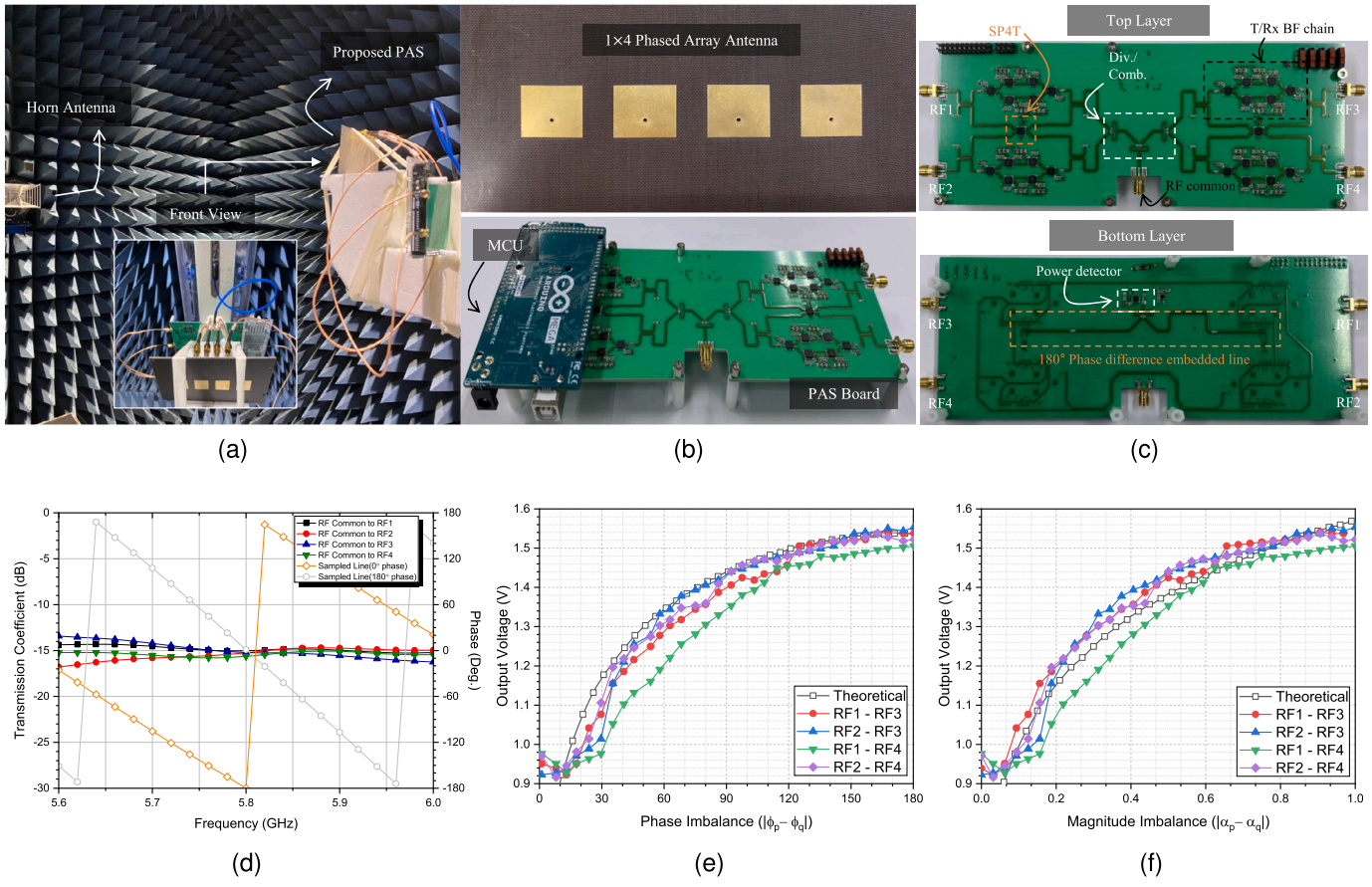

Fig. 4. (a) Measurement environment before and after the proposed built-in calibration. (b) Implementation of a 1×4 phased array antenna and PAS board with an MCU. (c) Detailed view of the PAS board with the proposed built-in calibration. Measured results of the (d) transmission coefficients and phase. The output voltage of the RF detector according to the (e) phase and (f) magnitude imbalance.

does not have a significant effect. The two signals are compared with a phase difference of 180°, and null is generated in the absence of an error. Also, if the receiver path of antenna 1 and antenna 3 is calibrating, the reference Rx signal is injected through the switch and two sampled lines. If the signals are coupled through the sampled lines after RF-chains, then it does not significantly affect the overall communication efficiency. Finally, the RF power detector was used to diagnose the position and depth of the null. The detector was selected in consideration of the dynamic range, and it receives an RF signal from the sampled lines and converts that into a voltage output. Also, the output is converted

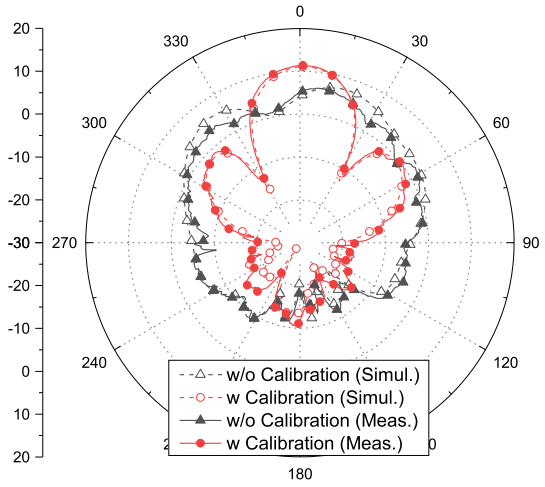

(a)

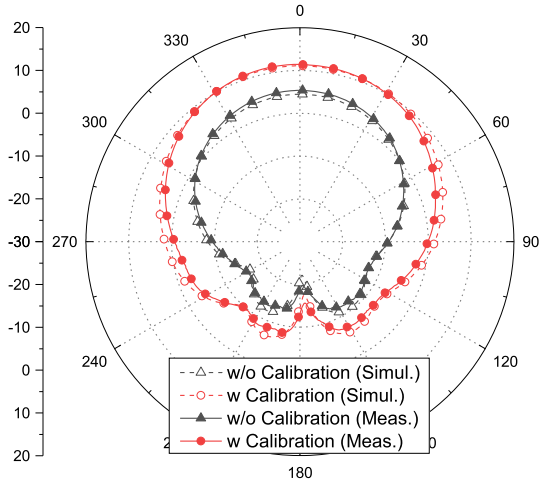

(b)

Fig. 5. The simulated and measured radiation patterns of 1×4 phased array antenna without and with the proposed calibration in the (a) E-plane and (b) H-plane.

through an analog-to-digital converter (ADC) and the output is monitored as a digital signal. Based on the digital signal, the microcontroller unit (MCU) performs phase and magnitude adjustment for calibration through serial peripheral interface (SPI) communication.

3. Experimental validation

The proposed built-in calibration in PAS was fabricated to simply verify the performance in transmitter mode, as shown in Fig. 4. A 1×4 phased array antenna was implemented with Taconic TLX-9 substrates having a dielectric constant of 2.5 and loss tangent of 0.0019. Here, the ground plane was 136 × 60 mm^2, corresponding to 2.63 λ_0 × 1.16 λ_0 at 5.8 GHz. Also, A PAS board was separately fabricated with different substrates, which is the Taconic RF-35 substrate having a dielectric constant of 3.5 and loss tangent of 0.0018. Fig. 4 (a) shows the measurement environment for comparing before and after calibration using the proposed built-in calibration, where An anechoic chamber and a reference horn antenna were used. Fig. 4 (b) shows the 1×4 phased array antenna for the beam pattern comparison, PAS board, and MCU for the control. Fig. 4 (c) provides a detailed view of the top and bottom layers on the PAS board with the proposed built-in calibration, where RF outputs 1-4, RF common, SP4T, divider/combiner, T/RF beamforming chains, power detector, and a 180° phase difference sampled line are described.

The PAS board was composed of a one-board by arranging the transmission/reception unit including the beamformer and the built-in calibration unit on the top and bottom layer, respectively. Therefore, compared to existing beamformers, the overall size of the board is the same even though the proposed built-in calibration function is included. The proposed architecture uses a Wilkinson Divider with good isolation characteristics between paths to be less affected by the leakage signal and perform accurate calibration. In addition, since only a few signals are sampled by using a directional coupler for built-in calibration, there is no significant effect on the transceiver signal. The entire integrated circuit (IC) is controlled by utilizing SPI communication (SPI Interface) to reduce the number of pins compared to the IC to be controlled between the PAS board and the MCU. When controlling the phase shifter and attenuator of the beamformer, it is designed to sequentially adjust and calibrate each IC element. Therefore, in this study, the MCU can be used to adjust the switch to determine the overall T/Rx mode, adjust the switch to select the antenna path, and read the signal of the power detector that passed through the ADC.

To verify the proposed built-in calibration, an RF-generated source of 0 dBm was fed to the RF common port. The measured transmission coefficients of the PAS are shown in Fig. 4 (d). Then, the measured transmission coefficients of the RF common to RF 1, 2, 3, and 4 were -15.0 dB, -15.2 dB, -15.2 dB, and -15.6 dB at 5.8 GHz, respectively. In addition, the measured phase of the two sampled lines is shown in Fig. 4 (d) as 181° at 5.8 GHz. Thus, the sampled lines were well fabricated at the center frequency because the ideal phase difference was designed as 180°. The output voltage was measured by the RF detector, as shown in Fig. 4 (e) and (f). The RF detector (LTC5582) was adopted with a wide dynamic range of 59 dB, which is within the ±1 dB linearity error. The minimum of the output voltage, which was combined with two 10-dB sampled signals from the main source, was the phase imbalance as shown in Fig. 4 (e).

In this paper, our proposed built-in calibration method was tested with four cases. The RF-chain of RF 1 can be compared with the RF-chains of RF 3 and 4. Similarly, the RF-chain of RF 2 can be compared with the RF-chains of RF 3 and 4. Ideal theoretical values with open square symbols can be compared with the measured values with imbalance. The measured phase imbalance of RF 1 - RF 3, RF 2 - RF 3, RF 1 - RF 4, and RF 2 - RF 4 were 10.51°, 1.12°, 13.04°, and 7.95°, respectively, which were the minimum point. The magnitude imbalance was tested in the same cases. The measured magnitude imbalances of RF 1 - RF 3, RF 2 - RF 3, RF 1 - RF 4, and RF 2 - RF 4 were 0.023, 0.006, 0.067, and 0.045, respectively. Errors in different states of the phase shifter and attenuator were compensated in advance. Finally, after the phase and magnitude imbalance was calibrated, the radiation pattern of the 1×4 phased array antenna was simulated and measured, as shown in Fig. 5. To verify the proposed built-in calibration in PAS, a 1×4 phased array antenna was simulated with the proposed calibration by the EM simulator (CST Studio Suite 2022). The imbalance signals of the implemented PAS board were fed to each antenna element without calibration, which then caused an abnormal radiation pattern. Conversely, the balance signals were fed with the proposed calibration; thus, an effective radiation pattern was generated. Also, the simulated radiation patterns of the H-plane without and with calibration are showed in Fig. 5 (b). The balanced radiation pattern was generated through the proposed calibration, and the measured results are in good agreement with the simulation results. The proposed calibration does not require a mixer and shows good performance at low cost.

Our built-in calibration for V2X communication was tested on an actual vehicle, as shown in Fig. 6. The PAS with the proposed built-in calibration was mounted inside the vehicle and its communication performance with a horn antenna outside the vehicle was tested, as shown in Fig. 6 (a). A PC (Samsung ATIV Book 9) calibrates the PAS board and controls the MCU for testing communication performance in the cen-

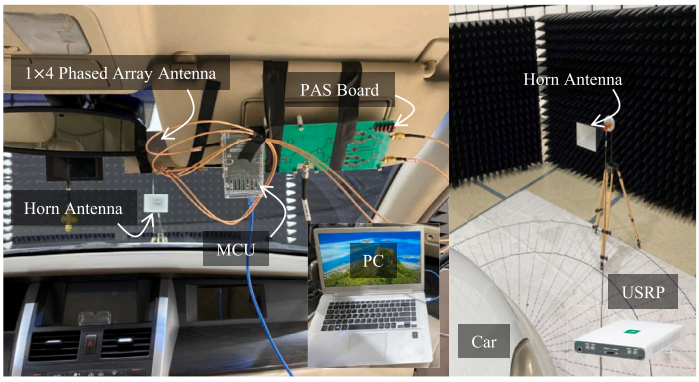

(a)

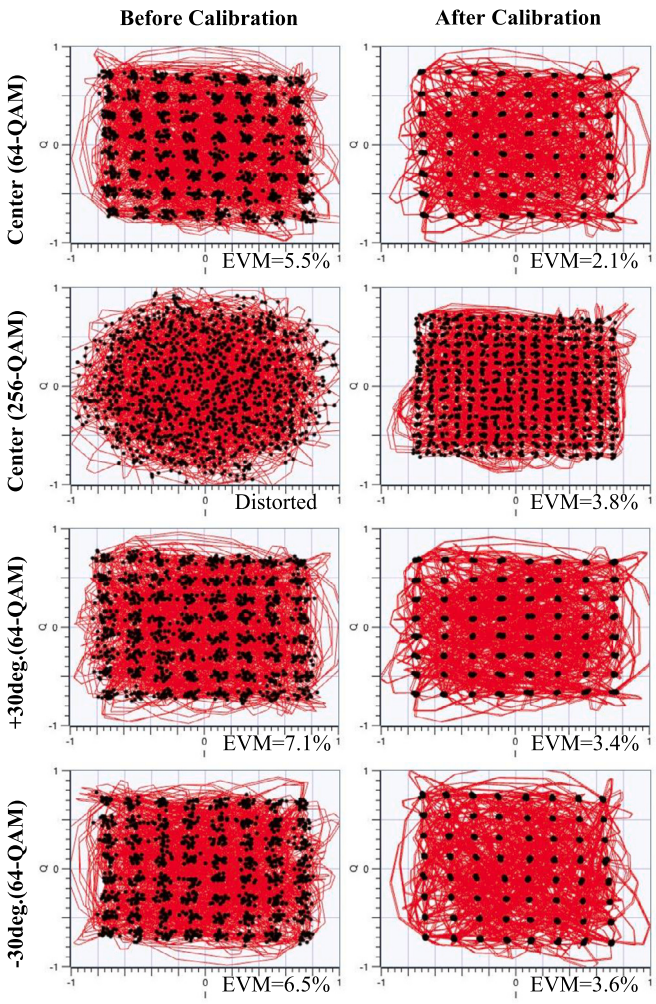

(b)

Fig. 6. (a) Photograph of the PAS with built-in calibration and experiment set up inside and outside a car. (b) Measured constellations and EVM versus center, +30 degree, and -30 degree directions from PAS for 64-QAM and 256-QAM before and after calibration.

ter, +30 degrees, and -30 degrees directions from the PAS. A USRP (NI 2954R) was used for the signal modulation, such as 64-QAM and 256-QAM with a sampling rate of 1M, 8 samples per symbol, and a symbol rate of 125k. The communication performance was tested before and after calibration, as shown in Fig. 6 (b), and as a result, a slight increase in error vector magnitude (EVM) was observed at the ±30 degrees directions, and higher order such as 64-QAM to 256-QAM showed high distorted constellations before calibration. We can verify that the proposed built-in calibration in PAS is useful for V2X communication. This guarantees PAS performance not only through factory default settings but also through periodic calibration when used in actual vehicles.

4. Conclusion

In this paper, a new built-in calibration in PAS for low cost and improved accuracy was proposed and verified at 5.8 GHz. In the proposed

built-in calibration, the process of detection and calibration is added for monitoring both phase and magnitude imbalances. The proposed method is both low complexity and low cost because it operates by detecting only the magnitude. Moreover, the proposed built-in calibration is based only on the sampled signal from the main source; therefore, no additional reference antenna or probe is required. Calibration can therefore be performed not only at factory default settings but also with periodic built-in calibration in actual vehicles. The proposed method uses minimum vector-sum tracking to improve accuracy, and showed good performance in a theoretical analysis. In addition, in vehicle experiments for V2X communication, the proposed built-in calibration delivered high-order modulated signals without distortion. Therefore, the proposed built-in calibration can be considered as a future solution for V2X communication applications.

Declaration of competing interest

The authors declare that they have no known competing financial interests or personal relationships that could have appeared to influence the work reported in this paper.

Acknowledgements

This research was supported in part by Institute for Information and Communications Technology Promotion (IITP) grant funded by the Korea government (MSIP) [2021-0-00151, A Development of W band Chirp Radar RFIC for Level Sensor], and in part by Korea Institute for Advancement of Technology (KIAT) grant funded by the Korea Government (MOTIE) (P0017011, HRD Program for Industrial Innovation).

References

[1] M. Kamran Ishfaq, et al., Compact wide-angle scanning multibeam antenna array for V2X communications, IEEE Antennas Wirel. Propag. Lett. 20 (11) (Nov. 2021) 2141–2145, https://doi.org/10.1109/LAWP.2021.3100349.
[2] J.-W. Kim, et al., Wide-angle scanning phased-array system using arc-shorted half elliptic elements, J. Electromagn. Waves Appl. 36 (Aug 2022) 261–271.
[3] H.-J. Dong, Y.-B. Kim, J. Joung, H.L. Lee, High gain and low-profile stacked magneto-electric dipole antenna for phased array beamforming, IEEE Access 8 (Sep. 2020) 180295–180304.
[4] B. Liu, J. Liu, N. Kato, Optimal beamformer design for millimeter wave dual-functional radar-communication based V2X systems, IEEE J. Sel. Areas Commun. 40 (10) (Oct. 2022) 2980–2993.
[5] H.-J. Dong, Y.-B. Kim, H.L. Lee, Reconfigurable quad-polarization switched beamforming antenna with crossed inverted-V array and dual-Butler matrix, IEEE Trans. Antennas Propag. 70 (4) (Apr. 2022) 2708–2716.
[6] Y.-B. Kim, H.-J. Dong, K.-S. Kim, H.L. Lee, Compact planar multipole antenna for scalable wide beamwidth and bandwidth characteristics, IEEE Trans. Antennas Propag. 68 (5) (May 2020) 3433–3442.
[7] Y.-B. Kim, S. Lim, H.L. Lee, Electrically conformal antenna array with planar multipole structure for 2-D wide angle beam steering, IEEE Access 8 (2020) 157261–157269.
[8] C. Balanis, Antenna Theory: Analysis and Design, Wiley, 2012.
[9] S. Kim, H.-W. Jo, J.-W. Kim, J.-I. Oh, J.-W. Yu, B. Ahn, Curved-retrodirective beamforming system to improve microwave power transmission efficiency in the Fresnel region, IEEE Int. Things J. (2023).
[10] C. Fulton, M. Yeary, D. Thompson, J. Lake, A. Mitchell, Digital phased arrays: challenges and opportunities, Proc. IEEE 104 (3) (March 2016) 487–503.
[11] C. Fulton, et al., Cylindrical polarimetric phased array radar: beamforming and calibration for weather applications, IEEE Trans. Geosci. Remote Sens. 55 (5) (May 2017) 2827–2841.
[12] I. Seker, Calibration methods for phased array radars, Proc. SPIE 8714 (2013).
[13] P.I. Muntianu, O. Breinbjerg, A 60 GHz first-order dual-port probe for spherical near-field antenna measurements, IEEE Antennas Wirel. Propag. Lett. 19 (9) (Sept. 2020) 1467–1470.
[14] J.K. Mulcahey, M.G. Sarcione, Calibration and diagnostics of the THAAD solid state phased array in a planar nearfield facility, in: Proc. Int. Symp. on Phased Array Systems and Technology, 1996, pp. 322–326.
[15] S. Mano, T. Katagi, A method for measuring amplitude and phase of each radiating element of a phased array antenna, Electron. Commun. Jpn. (1982) 58–64.
[16] C.-N. Hu, A novel method for calibrating deployed active antenna arrays, IEEE Trans. Antennas Propag. 63 (4) (Apr. 2015) 1650–1657.
[17] E. Sippel, M. Lipka, J. Geiß, M. Hehn, M. Vossiek, In-situ calibration of antenna arrays within wireless locating systems, IEEE Trans. Antennas Propag. 68 (4) (Apr. 2020) 2832–2841.
[18] L. Kong, X. Xu, Calibration of a polarimetric MIMO array with Horn elements for near-field measurement, IEEE Trans. Antennas Propag. 68 (6) (Jun. 2020) 4489–4501.
[19] Y. Cao, A.B. Ayed, J. Xia, S. Boumaiza, Uniformly distributed near-field probing array for enhancing the performance of 5G millimeter-wave beamforming transmitters, IEEE Microw. Wirel. Compon. Lett. 31 (6) (Jun. 2021) 823–826.
[20] H.-J. Yoon, B.-W. Min, Improved rotating-element electric-field vector method for fast far-field phased array calibration, IEEE Trans. Antennas Propag. 69 (11) (Nov. 2021) 8021–8026.
[21] Y. Wang, et al., Effect of temperature on electromagnetic performance of active phased array antenna, Electronics 9 (July 2020).
[22] A. Tsuchiya, H. Sugama, N. Hidaka, K. Miyamoto, S. Tsujino, O. Hashimoto, Temperature dependence of complex permittivity for polyimide film used in flexible printed circuit in microwave band, in: 2011 International Conference on Electromagnetics in Advanced Applications, Turin, Italy, 2011, pp. 417–420.
[23] T. Takahashi, N. Nakamoto, M. Ohtsuka, T. Aoki, Y. Konishi, I. Chiba, M. Yajima, On-board calibration methods for mechanical distortions of satellite phased array antennas, IEEE Trans. Antennas Propag. 60 (3) (Mar. 2012) 1362–1372.
[24] S.C. Chae, H.W. Jo, J.I. Oh, G. Kim, J.W. Yu, Coupler integrated microstrip patch linear phased array for self-calibration, IEEE Antennas Wirel. Propag. Lett. 19 (9) (Sept. 2020) 1615–1619.
[25] H. Steyskal, J.S. Herd, Mutual coupling compensation in small array antennas, IEEE Trans. Antennas Propag. 38 (12) (Dec. 1990) 1971–1975.
[26] H.M. Aumann, A.J. Fenn, F.G. Willwerth, Phased array antenna calibration and pattern prediction using mutual coupling measurements, IEEE Trans. Antennas Propag. 37 (7) (1989) 844–850.
[27] A. Nafe, K. Kibaroglu, M. Sayginer, G.M. Rebeiz, An in-situ self-test and self-calibration technique utilizing antenna mutual coupling for 5G multi-beam TRX phased arrays, in: 2019 IEEE MTT-S Int. Microw. Symp. (IMS), 2019, pp. 1229–1232.
[28] J. del Castillo, S. Sánchez, R. de Porras, A. Pedreira, J.R. Larrañaga, L-band digital array radar demonstrator for next generation multichannel SAR systems, IEEE J. Sel. Top. Appl. Earth Obs. Remote Sens. 8 (11) (Nov. 2015) 5007–5014.
[29] Kuan-Min Lee, Ruey-Shi Chu, Sien-Chang Liu, A built-in performance-monitoring/fault isolation and correction (PM/FIC) system for active phased-array antennas, IEEE Trans. Antennas Propag. 41 (11) (Nov. 1993) 1530–1540.
[30] O. Inac, D. Shin, G.M. Rebeiz, A phased array RFIC with built-in self-test capabilities, IEEE Trans. Microw. Theory Tech. 60 (1) (Jan. 2012) 139–148.
[31] S.Y. Kim, O. Inac, C.-Y. Kim, D. Shin, G.M. Rebeiz, A 76–84-GHz 16-element phased-array receiver with a chip-level built-in self-test system, IEEE Trans. Microw. Theory Tech. 61 (8) (Aug. 2013) 3083–3098.
[32] T. Kanar, G.M. Rebeiz, A 2-15 GHz built-in-self-test system for wide-band phased arrays using self-correcting 8-state I/Q mixers, in: 2016 IEEE MTT-S International Microwave Symposium (IMS), San Francisco, CA, USA, 2016, pp. 1–4.
[33] S.Y. Kim, O. Inac, C.-Y. Kim, G.M. Rebeiz, A 76–84 GHz 16-element phased array receiver with a chip-level built-in-self-test system, in: 2012 IEEE Radio Frequency Integrated Circuits Symposium, Montreal, QC, Canada, 2012, pp. 127–130.
[34] O. Inac, F. Golcuk, T. Kanar, G.M. Rebeiz, A 90–100-GHz phased-array transmit/receive silicon RFIC module with built-in self-test, IEEE Trans. Microw. Theory Tech. 61 (10) (Oct. 2013) 3774–3782.
[35] D. Chen, et al., A Ku-band 8-element phased-array transmitter with built-in-self-test capability, in: 2018 IEEE/MTT-S International Microwave Symposium - IMS, Philadelphia, PA, USA, 2018, pp. 610–612.
[36] Y. Yu, et al., A Ku-band eight-element phased-array transmitter with built-in self-test capability in 180-nm CMOS technology, IEEE Trans. Very Large Scale Integr. (VLSI) Syst. 30 (6) (June 2022) 694–705.
[37] Y. Wang, et al., A 39-GHz 64-element phased-array transceiver with built-in phase and amplitude calibrations for large-array 5G NR in 65-nm CMOS, IEEE J. Solid-State Circuits 55 (5) (May 2020) 1249–1269.
[38] S. Zeinolabedinzadeh, et al., A W-band SiGe transceiver with built-in self-test, in: 2019 IEEE 19th Topical Meeting on Silicon Monolithic Integrated Circuits in RF Systems (SiRF), Orlando, FL, USA, 2019, pp. 1–4.
[39] T. Takahashi, Y. Konishi, I. Chiba, A novel amplitude-only measurement method to determine element fields in phased arrays, IEEE Trans. Antennas Propag. 60 (7) (Jul. 2012) 3222–3230.
[40] R. Long, J. Ouyang, F. Yang, W. Han, L. Zhou, Fast amplitude-only measurement method for phased array calibration, IEEE Trans. Antennas Propag. 65 (4) (Apr. 2017) 1815–1822.
[41] Z. Wang, F. Zhang, H. Gao, O. Franek, G.F. Pedersen, W. Fan, Over-the-air array calibration of mmWave phased array in beam-steering mode based on measured complex signals, IEEE Trans. Antennas Propag. 69 (11) (Nov. 2021) 7876–7888.
[42] T. Takahashi, Y. Konishi, S. Makino, H. Ohmine, H. Nakaguro, Fast measurement technique for phased array calibration, IEEE Trans. Antennas Propag. 56 (7) (July 2008) 1888–1899.
[43] S. Kim, H.-J. Dong, J.-W. Yu, H.L. Lee, Phased array calibration system with high accuracy and low complexity, Alex. Eng. J. 69 (Apr. 2023) 759–770.